



Simulations of Thermal Softening in Large Strain Thermoplasticity

Balbina WCISŁO

Institute for Computational Civil Engineering
Faculty of Civil Engineering
Cracow University of Technology
Warszawska 24, 31-155 Kraków, Poland
e-mail: bwcislo@L5.pk.edu.pl

This paper deals with numerical simulations of the thermoplastic behaviour of isotropic materials undergoing large deformations. The attention is focused on the constitutive modelling of thermal softening understood here as a reduction of the plastic strength with increasing temperature. Different concepts of thermal softening embedded in the plasticity function are considered, in particular, the reduction of the total yield strength, its initial value or the hardening part. Moreover, apart from linear dependencies between temperature and the yield strength, the formulation involving function arc tangent is proposed. The analysed models are numerically tested in the finite element environment *AceFEM* using subroutines generated with the *AceGen* code generator. In particular, shear banding in an elongated rectangular plate with imperfection in plain strain conditions is investigated.

Key words: large strains, thermoplasticity, thermal softening.

1. INTRODUCTION

When a material experiences extreme loading it initially deforms uniformly and from some point strains localise in a narrow zone while the rest of the material experiences unloading. The phenomenon called strain localisation, which is a precursor of material fracture, can have three sources: material degradation (e.g. plasticity with softening or damage), geometrical softening (related to the decreasing cross-section of elongated sample while the plasticity function limits stresses) or temperature-induced softening.

It is well recognised that material parameters change with temperature. Usually, the increase of temperature for energetic materials [3] causes decreasing elastic stiffness of the material and a reduction of the yield strength.

Many materials, especially metals, generate heat resulting from the dissipation of energy when sustain plastic strains. Thus, even in the absence of external sources of heat, temperature of the sample can increase during deformation and cause softening of the material. If localisation occurs, then in the band with large plastic strains the heat generation is the highest, and the yield strength is reduced progressively. It can not be neglected that in a material subjected to non-uniform distribution of temperature, heat flows through the material tending to homogeneous state. Admittedly, heat conduction influences the localisation behaviour but its regularising properties depend on time in contrast to standard gradient-enhanced models. In fact, even for a high value of heat conduction coefficient assumed for a material, the process can be treated as nearly adiabatic for deformation occurring in a very short time. The effect of heat conduction on localisation phenomena was investigated in several papers, e.g. [1, 4] or [7].

In this paper special attention is focused on the modelling of thermal softening incorporated in the plasticity function. This modelling can take various forms, see e.g. [8] or [6], and it may reduce the total yield strength, its initial threshold or hardening contribution using linear or more complex functions as arc tangent function proposed in this paper. Thus, the aim of this research is to investigate the influence of the different thermal softening functions on the material behaviour and strain localisation. Especially, the question to be answered is how strongly the material response depends on the degradation of the individual parts of the yield strength. The analysis is based on numerical simulations of shear banding in an elongated plate in plane strain conditions.

The paper is laid out as follows. In Sec. 2, the material model of large strain thermo-elastoplasticity accounting for thermal softening is presented. Moreover, different forms of temperature influence on the yield strength are specified. In Sec. 3, the results of numerical verification for the presented models are included and, finally, the paper ends with some remarks.

2. MODEL DESCRIPTION

2.1. Constitutive relations and governing equations

The material model analysed in the paper is based mainly on the formulation of isotropic large strain thermoplasticity presented in [5]. The thorough presentation of the final model is included in [7], thus, in this paper only the general description is presented.

The analysed thermomechanical model is based on the multiplicative decomposition of the deformation gradient

$$(2.1) \quad \mathbf{F} = \mathbf{F}^\theta \mathbf{F}^e \mathbf{F}^p,$$

where $\mathbf{F}^\theta = \exp[\alpha_T(T - T_0)]\mathbf{I}$ is a part related to thermal expansion (α_T denotes the coefficient of linear thermal expansion, \mathbf{I} is the second-order identity tensor, T_0 and T are the reference and absolute temperatures, respectively), \mathbf{F}^e is an elastic contribution, and \mathbf{F}^p involves the irreversible (plastic) deformation.

The state of the material is described by the Helmholtz free energy potential that is assumed in the following decoupled form [8]

$$(2.2) \quad \psi(\mathbf{b}^e, T, \gamma) = \psi^e(\mathbf{b}^e) + \psi^\theta(T) + \psi^p(\gamma),$$

which distinguishes the elastic, thermal and plastic parts as in [7]. The quantity $\mathbf{b}^e = \mathbf{F}^e(\mathbf{F}^e)^T$ is the elastic left Cauchy-Green tensor and γ is a scalar plastic strain measure.

The yield function that governs the plastic regime is assumed in the following form

$$(2.3) \quad F^p(\boldsymbol{\tau}, \gamma, T) = f(\boldsymbol{\tau}) - \sqrt{2/3}\sigma_y(\gamma, T) \leq 0.$$

The equivalent stress function $f(\boldsymbol{\tau})$ is a measure of Kirchhoff's stress tensor $\boldsymbol{\tau} = 2[\partial\psi^e/\partial\mathbf{b}^e]\mathbf{b}^e$ (here Huber-Mises-Hencky) and $\sigma_y(\gamma, T)$ denotes the yield strength, which is discussed in the next Section, including strain hardening and thermal softening. The description of plasticity is completed with the evolution law for \mathbf{b}^e and the loading-unloading conditions assumed as in [7].

The constitutive relation for the Kirchhoff heat flux is the standard Fourier's law defined in the current configuration: $\mathbf{q} = -k\nabla T$, where k denotes the heat conductivity.

The governing equations for the coupled problem cover the balance of linear momentum (here, a static case without body forces is considered) and the conservation of energy, which is expressed in temperature form [5]. The equations are written as follows:

$$(2.4) \quad J\text{div}(\boldsymbol{\tau}/J) = \mathbf{0}, \quad \rho c \frac{\partial T}{\partial t} = J\text{div}(-\mathbf{q}/J) + \mathcal{R}.$$

In the first equation, $\text{div}(\cdot)$ denotes divergence in spatial description and $J = \det(\mathbf{F})$, whereas quantities in the energy balance equation are the following: c – heat capacity, ρ – density, t – time, \mathbf{q} – Kirchhoff's heat flux. The variable \mathcal{R} represents a heat source due to plastic dissipation and is used here in a simplified form with the Taylor-Quinney factor χ : $\mathcal{R} = \sqrt{2/3}\chi\sigma_y\dot{\gamma}$. All differential equations are completed with proper boundary conditions, see [7].

It can be noted that in the presented large strain model a full thermomechanical coupling is adopted, i.e., the model includes thermal expansion, dependence of material parameters on temperature, plastic self-heating incorporated in the energy balance and the influence of deformation on the heat flux.

2.2. Thermal softening variants

As it was mentioned, the main attention in this paper is paid to the modelling of thermal softening embedded in the plasticity function. In the work three main types of thermal softening are distinguished depending on whether the temperature increase reduces the total yield strength, its initial threshold or the hardening component.

Firstly, the mechanical part of the yield strength involving strain hardening is reduced with a thermal factor, see also [8],

$$(2.5) \quad \sigma_y(\gamma, T) = \sigma_y^M(\gamma) \cdot \sigma_y^T(T).$$

In this work, the mechanical part σ_y^M includes linear and saturation-type strain hardening

$$(2.6) \quad \sigma_y^M(\gamma) = \sigma_{y0} + \sqrt{2/3}H_i\gamma + [\sigma_{y\infty} - \sigma_{y0}] \left[1 - e^{-\sqrt{2/3}\delta\gamma} \right],$$

where σ_{y0} denotes the initial yield strength and H_i , $\sigma_{y\infty}$, δ are the parameters which describe hardening.

In turn, thermal softening part $\sigma_y^T(T)$ can be, in the simplest case, a linear function of T

$$(2.7) \quad \sigma_y^T(T) = 1 - H_T[T - T_0],$$

where H_T is a thermal softening modulus. This model is called *TS1 lin* in subsequent simulations. Note that, for a sufficiently high increase of temperature, the yield strength can achieve negative values, which is obviously inconsistent with the physical properties of materials. Thus, the application of linear thermal softening is limited. Alternatively, the thermal softening contribution can be defined using arc tangent function and the following form (called further *TS1 atan*) is proposed

$$(2.8) \quad \sigma_y^T(T) = -A \cdot \arctan [B \cdot [T - T_0] - C] + D,$$

where A , B , C , D are material parameters. The advantage of formulation (2.8) is that a wider range of temperature increase can be properly covered in simulations.

Secondly, the constant initial yield strength (independent of temperature) is assumed in the model (*TS2 lin*). Thus, the yield strength can be formulated in the following way:

$$(2.9) \quad \sigma_y(\gamma, T) = \sigma_{y0} + \sigma_y^{MT}(\gamma, T).$$

The strain hardening – thermal softening function $\sigma_y^{MT}(\gamma, T)$ is assumed in such a way that material parameters H_i and $\sigma_{y,\infty}$ depend on temperature (here, linear dependencies with modules H_{TH} and $H_{T\sigma_\infty}$ are adopted)

$$(2.10) \quad \sigma_y^{MT} = \sigma_{y0} + \sqrt{2/3}H_i(T)\gamma + [\sigma_{y\infty}(T) - \sigma_{y0}] \left[1 - e^{-\sqrt{2/3}\delta\gamma}\right],$$

$$(2.11) \quad \begin{aligned} H_i(T) &= H_i(T_0) [1 - H_{TH}(T - T_0)], \\ \sigma_{y\infty}(T) &= \sigma_{y\infty}(T_0) [1 - H_{T\sigma_\infty}(T - T_0)]. \end{aligned}$$

Thirdly, following the assumption often made in thermoplasticity, see also, e.g., [5], the change of temperature acts only on the initial value of the plastic strength (model *TS3 lin*)

$$(2.12) \quad \sigma_y(\gamma, T) = \sigma_{y0}(T) + \sigma_y^{hard}(\gamma),$$

whereas the hardening function depends only on the plastic strain measure. In numerical simulations the hardening part involves linear and saturation-type contribution as in Eq. (2.6), whereas the initial yield strength here depends on temperature linearly:

$$(2.13) \quad \sigma_{y0}(T) = \sigma_{y0}(T_0) [1 - H_{T\sigma_0}(T - T_0)].$$

3. NUMERICAL TESTING

Numerical simulations are performed using symbolic-numerical packages *Ace* working in *Wolfram Mathematica* environment. The user-supplied subroutines for the finite element method are developed using automatic *AceGen* code generator. The broad discussion on the implementation of the large strain thermo-plasticity within finite element method is discussed in [7]. The finite element codes are prepared for the general three-dimensional case. This allows for the wider range of possible simulations.

A series of computational tests for an elongated rectangular plate in plane strain conditions are performed. The analysed specimen has dimensions of $0.20 \times 0.10 \times 0.0025$ m and a square imperfection of in-plane dimensions 0.005×0.005 m in the center. Due to symmetry of the sample, the implementation is performed for one-quarter of the specimen, which is elongated with enforced displacement of maximum value 0.02 m during 1 s. The remaining mechanical boundary conditions correspond to symmetry and plane strain requirements. The insulation is assumed on the entire surface (adiabatic boundary conditions).

In all simulations, three-dimensional hexahedral finite elements are used. All fields are interpolated with the linear shape functions, and *F-bar* enhancement

preventing volumetric locking in plasticity [2] is incorporated. However, it should be mentioned that this modification of the deformation gradient causes small non-zero strains in the thickness direction, even though the related displacements are zero. The plate is discretised with uniform meshes: coarse $40 \times 20 \times 1$ (mesh 1) and fine $80 \times 40 \times 1$ (mesh 2).

The material parameters for the constitutive model applied in the simulations are as follows: hyperelasticity: $K = 164.2\text{e}9 \text{ N/m}^2$, $G = 80.19\text{e}9 \text{ N/m}^2$, plasticity function: $\sigma_{y0} = 0.45\text{e}9 \text{ N/m}^2$, $\sigma_{y\infty} = 0.6\text{e}9 \text{ N/m}^2$, $H_i = 129\text{e}6 \text{ N/m}^2$, $\delta = 16.93$, density: $\rho = 7.8\text{e}3 \text{ kg/m}^3$, and thermal parameters: $k = 100 \text{ J/(s} \cdot \text{K} \cdot \text{m)}$, $c = 460 \text{ J/(kg} \cdot \text{K)}$, $\alpha_T = 12\text{e}-6 \text{ K}^{-1}$, $T_0 = 293.15 \text{ K}$, $\chi = 0.9$. The imperfection is understood here as a reduction of the initial yield strength to $\sigma_{y0,imp} = 0.8\sigma_{y0}$. The nonlinear problem is solved with an iterative Newton-Raphson procedure using adaptive time steps.

Firstly, the numerical simulations are performed for the three presented variants of thermal softening involving linear dependencies. Thus, models *TS1 lin*, *TS2 lin*, *TS3 lin* are tested with the following material parameter values: $H_T = H_{T\sigma 0} = H_{TH} = H_{T\sigma\infty} = 0.005$. In Fig. 1, the load-displacement diagram for the analysed cases is presented. It can be observed that up to the peak point the diagrams for all models are very close and later a stiffer response is noticed for the model, in which thermal softening acts on the initial yield strength (*TS3 lin*). The results obtained for the latter model are identical for both considered meshes and the shape of the diagram suggests a diffuse mode of localisation, which is confirmed in the lower picture in Fig. 2. Moreover, for models *TS1 lin* and *TS2 lin* the response is close and the larger inclination of the diagram is observed in the post-peak regime than for *TS3 lin*. For the first two variants, the strains localise in a shear band, see the upper picture in Fig. 2. The deformed mesh for *TS2 lin* with temperature distribution is practically identical as for *TS1 lin*, and due to this it is not presented here (the only difference is the maximum increase of temperature which is slightly higher for *TS2 lin* and equals

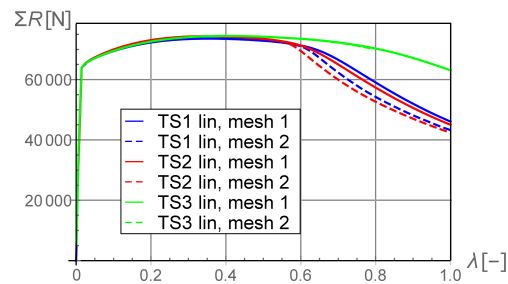


FIG. 1. Sum of reactions vs enforced displacement multiplier for thermoplastic material with different thermal softening functions.

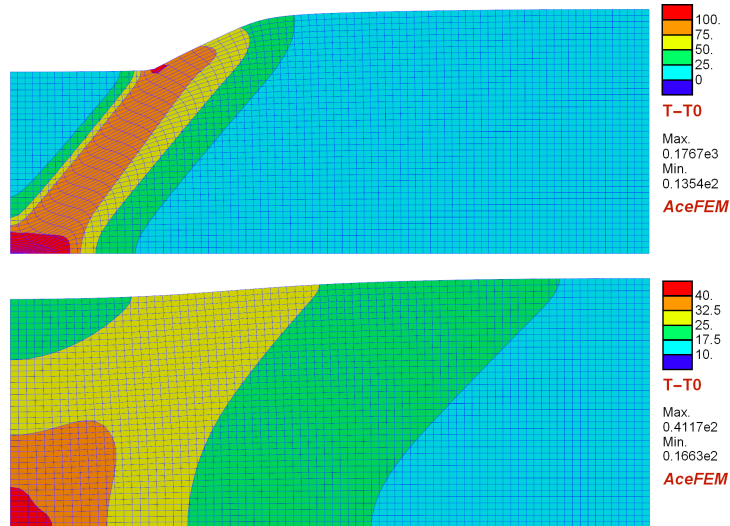


FIG. 2. Deformed mesh with temperature distribution at the end of elongation process for thermal softening modelled with *TS1 lin* (upper) and *TS3 lin* (lower).

180 K). Note that, despite slight differences in the load-displacement diagrams for mesh 1 and mesh 2, the band has a specified width that does not seem to be mesh-dependent. It can be concluded that in this case heat conduction regularises the response of the material sufficiently. Furthermore, it can be seen in Fig. 2 that the differences in temperature distribution for *TS1 lin* and *TS3 lin* are significant (the maximum increase for the localised mode is more than four times higher than for the diffuse one).

Secondly, numerical experiments are performed for linear thermal softening model *TS1 lin* to compare the response of the sample for different values of modulus $H_T = 0.002 \text{ K}^{-1}$ and $H_T = 0.005 \text{ K}^{-1}$. The load-displacement diagrams for both cases are put together in Fig. 3. It can be observed that the difference is not only quantitative but qualitative as well. At the end of elongation, for the lower value of thermal softening modulus a diffuse form of localisation in the form of a neck is observed, see the deformed mesh in Fig. 3, with identical responses for the two adopted discretisations. For comparison, the final configuration with shear band for $H_T = 0.005 \text{ K}^{-1}$ is presented in the upper picture in Fig. 2.

Finally, a comparison of the results obtained for models *TS1 lin* and *TS1 atan* is performed. Now the following material parameters are assumed: for function *TS1 lin*: $H_T = 0.005 \text{ K}^{-1}$, for *TS1 atan*: $A = 0.366$, $B = 0.030 \text{ K}^{-1}$, $C = 2.50$ and $D = 0.536$. For a better recognition of the adopted functions, in the left diagram in Fig. 4 the relation between the initial yield strength and the increase of temperature (with respect to room temperature $T_0 = 293.15 \text{ K}$) is

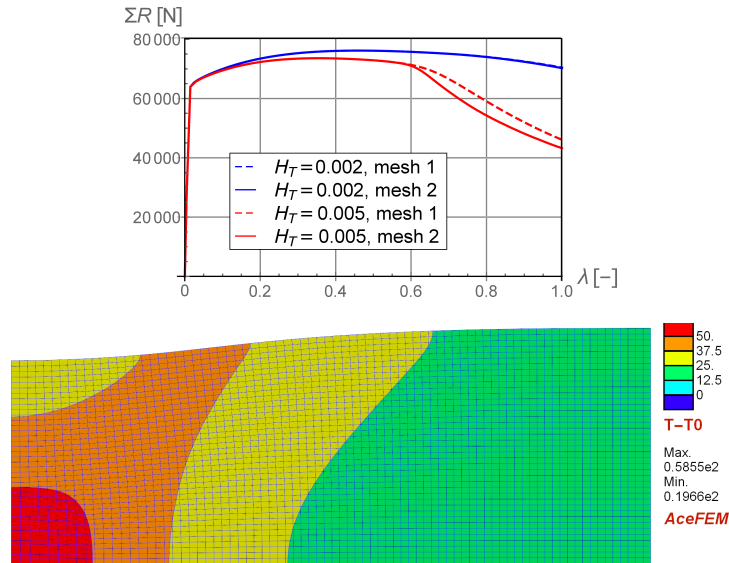


FIG. 3. Sum of reactions vs enforced displacement multiplier for thermoplastic material with linear thermal softening for different values of modulus H_T (upper) and deformed mesh at the end of elongation for $H_T = 0.002 \text{ K}^{-1}$ (lower).

depicted. It can be observed in the right picture in Fig. 4 that the results for *TS1 atan* differ significantly from the response for linear function *TS1 lin* in the post-peak range. The material loses its stability much later and the diagrams descend then rapidly. What is more, for model *TS1 atan* the diagrams in the post-peak regime for the two adopted meshes differ more than for the linear model and the strains localise in bands of different widths, which can be noticed in the deformed sample plots presented in Fig. 5. For mesh 2 (the lower picture), the localisation zone is narrower and a higher temperature increase is observed.

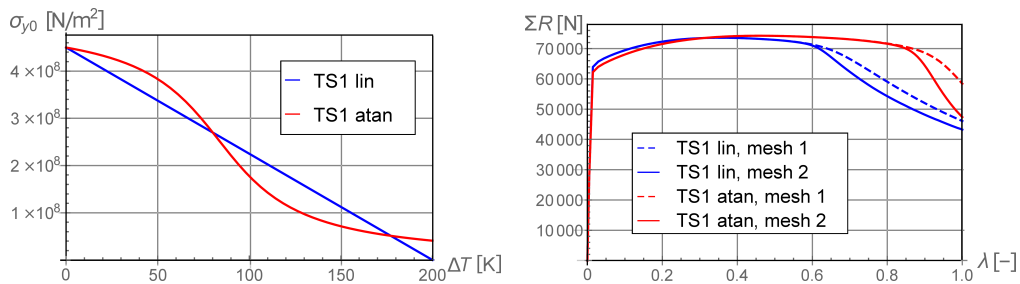


FIG. 4. Initial yield strength (on the right), and sum of reactions vs enforced displacement multiplier (on the left) for thermoplastic material with different thermal softening functions.

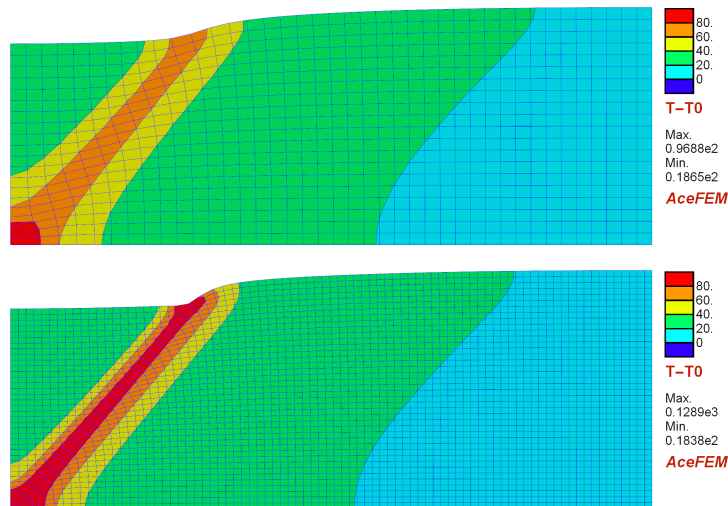


FIG. 5. Deformed meshes with temperature distribution for thermoplastic material with thermal softening function $TS1 \text{ atan}$.

4. CONCLUSION

In this paper, the large strain thermoplastic material behaviour has been investigated with the special attention paid to the formulation of thermal softening influencing the yield strength. Three models have been identified in the work and numerically studied using the finite element method. In particular, the temperature change can influence the total yield strength, the hardening contribution or the initial value of the plasticity threshold.

The numerical simulations performed for the elongated plate in plane strain conditions reveal that the form of thermal softening does not influence significantly the response of the sample in the pre-peak regime. However, if the initial yield strength is subjected to thermal softening only then the response of the sample in the post-peak range is stiffer and less susceptible to a loss of stability. Moreover, depending on the magnitude of the linear thermal softening modulus for the same model different modes of strain localisation can be observed (diffused or localised). Finally, an alternative to linear softening formulation involving the arc tangent function has been tested which is physically more justified (yield strength cannot achieve negative value). However, although the material parameters for arc tangent function are adopted in such a way that the relation between the initial yield strength and the temperature increase is close to the linear model, the response in the post peak-regime for this case is significantly different. It is important that the choice of thermal softening function highly influences not only the final deformation of the sample but the temperature distribution as well.

Summarising, the research provides new developments involving:

- numerical analysis of different thermal softening models in large strain thermoplasticity in the context of strain localisation,
- proposal and examination of thermal softening described with the arc tangent function.

ACKNOWLEDGMENT

The author acknowledges valuable discussions on the research with Prof. J. Pamin (Cracow University of Technology) and also with Prof. A. Menzel (TU Dortmund, Germany/Lund University, Sweden) who proposed to represent thermal softening with an arc tangent function.

The research was supported by the National Science Centre of Poland [grant number 2014/15/B/ST8/01322].

REFERENCES

1. BATRA R.C., KIM C.H., *Effect of thermal conductivity on the initiation, growth and bandwidth of adiabatic shear bands*, International Journal of Engineering Science, **29**(8): 949–960, 1991, doi: 10.1016/0020-7225(91)90168-3.
2. DE SOUZA NETO E.A., PERIC D., OWEN D.R.J., *Computational methods for plasticity. Theory and applications*, John Wiley & Sons Ltd, Chichester, UK, 2008.
3. HOLZAPFEL G.A., *Nonlinear solid mechanics: A continuum approach for engineering*, John Wiley & Sons Ltd, Chichester, 2000.
4. LEMONDS J., NEEDLEMAN A., *Finite element analyses of shear localization in rate and temperature dependent solids*, Mechanics of Materials, **5**(4): 339–361, 1986, doi: 10.1016/0167-6636(86)90039-6.
5. SIMO J.C., MIEHE C., *Associative coupled thermoplasticity at finite strains: Formulation, numerical analysis and implementation*, Computer Methods in Applied Mechanics and Engineering, **98**(1): 41–104, 1992, doi: 10.1016/0045-7825(92)90170-O.
6. SIMO J.C., *Numerical analysis and simulation of plasticity*, [in:] Ciarlet P.G., Lions J.L. [Eds.], *Handbook of numerical analysis. Numerical methods for solids*, Part 3, Volume VI, pp. 183–499, Elsevier Science, Boca Raton, 1998.
7. WCISŁO B., PAMIN J., *Local and non-local thermomechanical modeling of elastic-plastic materials undergoing large strains*, International Journal for Numerical Methods in Engineering, **65**, 2016 (in print), doi: 10.1002/nme.5280.
8. WRIGGERS P.A., MIEHE C., KLEIBER M., SIMO J.C., *On the coupled thermomechanical treatment of necking problems via finite element methods*, International Journal for Numerical Methods in Engineering, **33**(4): 869–883, 1992, doi: 10.1002/nme.1620330413.

Received October 18, 2016; accepted version November 10, 2016.
